Supplementary Information

Ultrasonic induced liquid-phase exfoliation boosts excellent performance of $Bi_{0.5}Sb_{1.5}Te_3$/PVDF thermoelectric films

Haotian Li,[a] Shaoqiu Ke,[a] Xiaoxiao Yu,[a] Haojun Zhang,[a] Xinyang Zhang,[a] Xiaolei Nie,[a,*] Wanting Zhu,[a] Ping Wei,[a, b,*] Wenyu Zhao,[a] Qingjie Zhang[a]

[a] *State Key Laboratory of Advanced Technology for Materials Synthesis and Processing, Wuhan University of Technology, Wuhan 430070, China*

[b] *Nanostructure research center, Wuhan University of Technology, Wuhan 430070, China*

* Corresponding authors: X. Nie (xiaoleinie@whut.edu.cn) or P. Wei (pingwei@whut.edu.cn)

S1. Structural characterization and property measurements

Structural characterization

The constituent phases of the $Bi_{0.5}Sb_{1.5}Te_3$/polyvinylidene fluoride (BST/PVDF) films were examined by powders X-ray diffraction (XRD, SmartLab, Rigaku Corporation, Tokyo, Japan) using Cu Kα radiation (λ= 0.154186 nm) source. The surface and cross-sectional morphology were characterized with field emission scanning electron microscope (FESEM, JEM-7500F, Nippon Electronics Corporation, Tokyo, Japan). The microstructures were characterized using electron probe micro-analyzer (EPMA, JXA-8230, Nippon Electronics Corporation, Tokyo, Japan).

Property measurements

The α and σ of all the samples in the range of 300-500 K were synchronously measured using the standard four probe method (CTA-3, Beijing Cryall Science and Technology Co., Ltd., Beijing, China) in a helium environment. Uncertainties are ±5-7% for σ and about ±5% for α. The traditional Vanderbilt Hall method was used to measure the Hall coefficient (R_H) of all the samples. The cooling performance of single-leg devices was measured using self-made instruments, with a DC power supply (Gwinstek, GPD-2303S) to provide working current, and high-precision T-type thermocouples (OMEGA Engineering INC.) to detect the temperature at both ends. All data was recorded by the acquisition module and LabVIEW program. The bending test was conducted using a flexible material and equipment testing system (FlexTest-TM-L, Huanan Nasheng Electronic Technology Co., Ltd., Huanan, China).

S2. The orientation factor (*F*) for BST

To quantitatively study the effect of UILPE on the BST films, the orientation factor (*F*) of BST along the (000*l*) surface was calculated by using the Lotgering method, [1]

$$F(X) = \left(P - P_0\right)/\left(1 - P_0\right) \quad (1)$$

$$P = \Sigma I(X)/\Sigma I(\text{hkil}) \qquad P_0 = \Sigma I_0(X)/\Sigma I_0(\text{hkil}) \quad (2)$$

$\Sigma I(X)$, $\Sigma I_0(X)$, $\Sigma I(\text{hkil})$ and $\Sigma I_0(\text{hkil})$ are the sum of (X) and (hkil) diffraction intensities of the

preferentially oriented sample and the BST (JCPDS 49-1713) standard card, respectively. P and P_0 are the ratios of the preferentially oriented sample and the BST (JCPDS 49-1713) standard card, respectively. The F of all samples were calculated using equation (1).

S3. The EPMA images of cross section of BST films

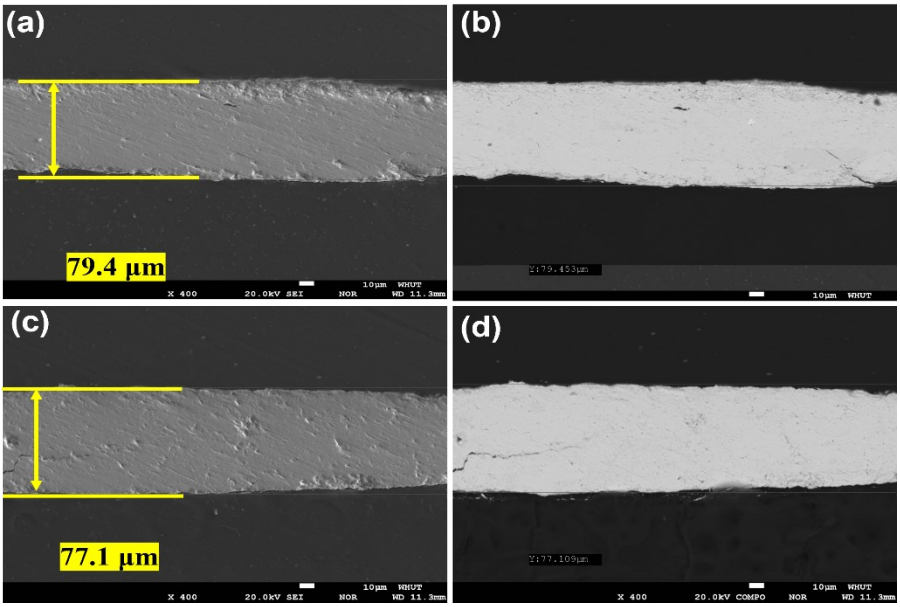

Fig. S1 EPMA images of cross section of BST films. (a) Secondary electron image and (b) backscattered electron image of the UILPE-BST/PVDF films. (c) Secondary electron image and (d) backscattered electron image of the BM-BST/PVDF films.

As can be seen from **Fig. S1**, the thickness of the UILPE-BST/PVDF film is 79.4 μm, while that of the BM-BST/PVDF film is 77.1 μm. It can be observed that there are some voids from the secondary electron image of the BM-BST/PVDF film (**Fig. S1c**), which is detrimental to the formation of conductive pathways.

S4. The microstructures of the fractured section of BST/PVDF films under different UILPE power

To further study the effect of UILPE power on the microstructures of the fractured section of BST/PVDF films, the FESEM images were shown in **Fig. S2**. In the BM-BST/PVDF films, the most of BST grains exhibit a random orientation (**Fig. S2a**), while those of UILPE-BST/PVDF films are arranged along the [000*l*] orientation as shown in **Fig. 2c, d and e.** As the power of UILPE increases, the layered BST grains enlarge, and the internal structure within the films become denser and more uniform. When the power is increased to 360 W, the $UILPE_{360W}$-BST/PVDF film exhibits the highest electrical conductivity and the best electrical transport performance. This enhancement in the internal structure's density and uniformity results in the high (000*l*) preferential orientation and more carrier transport channels, consequently increasing the carrier mobility (μ). However, an

excessive power can sharply reduce the size of BST grains, which is detrimental to the continued increase of μ.

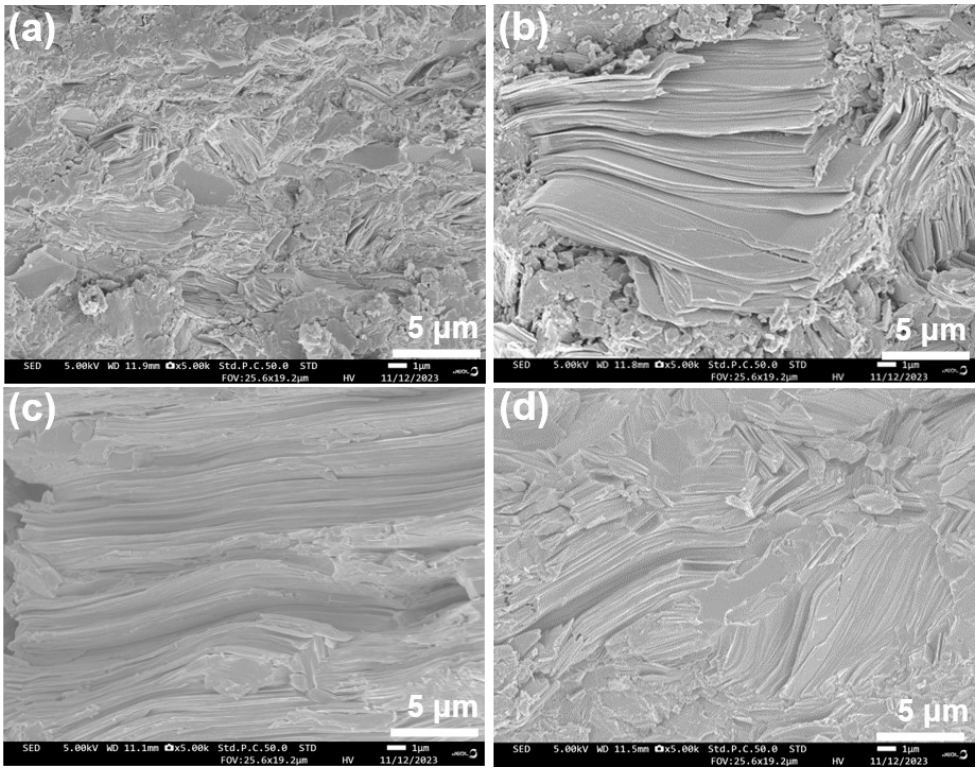

Fig. S2 Microstructures of the fractured section of the BST/PVDF films. (a) BM-BST/PVDF films, (b) UILPE$_{240\ W}$-BST/PVDF films, (c) UILPE$_{360\ W}$-BST/PVDF films and (d) UILPE$_{480\ W}$-BST/PVDF films.

S5. Comparison of TE performance

Table S1 Comparison of TE performance of other reported films and UILPE$_{360\ W}$-BST/PVDF film at room temperature[2-9]

Materials	Methods	σ (10^4 S·m^{-1})	α (μV·K^{-1})	PF (mW K^{-2} m^{-1})	Ref
Bi_2Te_3/PEDOT	Vapor deposition + VPP	4.83	168	1.36	4
Bi_2Te_3	Magnetron co-sputtering	3.68	184	1.25	5
Ag_2Se	Wet-chemical process + HP	9.2	-143	1.88	6
$Bi_{0.4}Sb_{1.6}Te_3$/Te	Screen-printing + sintering	7.21	204	3.00	7
$Bi_{0.5}Sb_{1.5}Te_3$	Screen-printing + HP	6.00	174	1.82	8
Ag_2Se/Se/PPy	Wet-chemical process + HP	10.64	-144	2.24	9
Sb_2Te_3/Te_x	Directional thermal diffusion	12.80	125	2.00	10
Ag_2Se	Wet-chemical process + HP	4.97	-140	0.99	11
UILPE$_{360\ W}$-BST/PVDF	**Screen-printing + HP**	**4.33**	**232**	**2.33**	**This work**

VPP = vapor phase polymerization, HP = Hot pressing, PPy = Polypyrrole, PVP = Polyvinylpyrrolidone

To better facilitate comparison of the room temperature TE performance of the flexible composite films, the TE performance of other reported TE flexible composite films were listed in **Table S1**. It can be seen that the TE films prepared in this study exhibit good TE performance compared to other TE films in this field.

S6. Flexibility performance of single-leg devices

The flexibility of the UILPE-BST/PVDF films was characterized by the FlexTest-TM-L testing system. The resistance ratio (R/R_0) at different bending radius and cycles before and after the bending test were recorded to evaluate the flexibility of the UILPE-BST/PVDF films. The initial internal resistance (R_0) of the film is 2.3 Ω. By real-time monitoring of the actual resistance R during the flexibility testing process, the R/R_0 of the UILPE-BST/PVDF films was calculated. As shown in **Fig. S3a**, when the bending radius (r) is reduced from 50 mm to 15 mm during the testing process, the R/R_0 of the UILPE-BST/PVDF films remains almost unchanged, indicating good flexibility. When the r decreases to 15 mm, the R/R_0 begins to increase. When the r is less than 10 mm, the R/R_0 increases sharply, indicating the occurrence of cracks inside the UILPE-BST/PVDF films and damage to its flexibility. To study the flexibility of UILPE-BST/PVDF films under bending cycles, bending tests were conducted within a r of 20 mm and the R/R_0 of the UILPE-BST/PVDF films was measured in real-time. From **Fig. S3b**, it can be seen that when the number of cycles is less than 8000, the R of the UILPE-BST/PVDF films remains almost unchanged. As the number of cycles increasing, R gradually increases, which is due to the formation of microcracks inside the UILPE-BST/PVDF films. When the number of cycles reaches 15000, R increases sharply, the film cracks, and flexibility is lost. By conducting flexibility tests on the UILPE-BST/PVDF films under different bending radius and cycle times, it's demonstrated that the UILPE-BST/PVDF films have good flexibility.

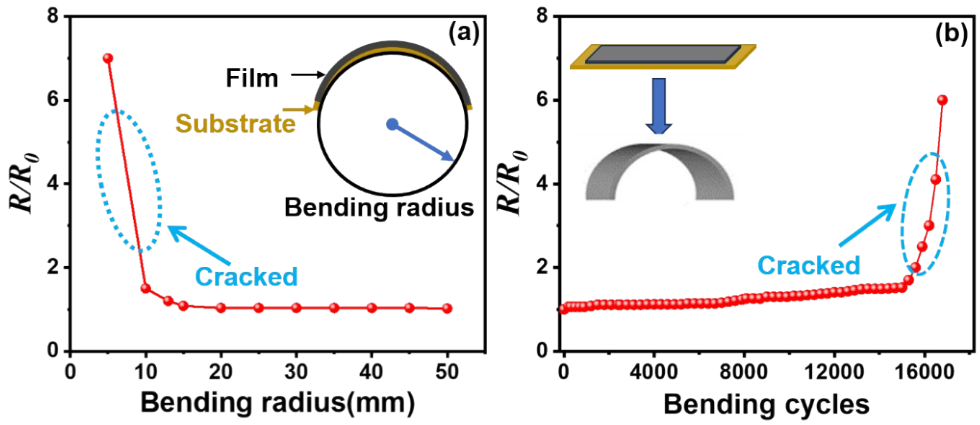

Fig. S3 Flexibility of the UILPE-BST/PVDF films. (a) Bending radius and (b) Bending cycles.

References

1. F. K. Lotgering, *Journal of Inorganic and Nuclear Chemistry*, 1959, **9**, 113-123.
2. L. Wang, Z. Zhang, Y. Liu, B. Wang, L. Fang, J. Qiu, K. Zhang and S. Wang, *Nature Communications*, 2018, **9**, 3817.
3. D. Qin, F. Pan, J. Zhou, Z. Xu and Y. Deng, *Nano Energy*, 2021, **89**, 106472.
4. C. Jiang, Y. Ding, K. Cai, L. Tong, Y. Lu, W. Zhao and P. Wei, *ACS Applied Materials & Interfaces*, 2020, **12**, 9646-9655.
5. T. Varghese, C. Dun, N. Kempf, M. Saeidi-Javash, C. Karthik, J. Richardson, C. Hollar, D. Estrada

and Y. Zhang, *Advanced Functional Materials*, 2019, **30**, 1905796.
6. P. Banerjee, J. Huang, R. B. Ambade, E. Jang, M. Saeidi-Javash, Y. Zhang and D. Madan, *Nano Energy*, 2021, **89**, 106482.
7. Y. Li, Q. Lou, J. Yang, K. Cai, Y. Liu, Y. Lu, Y. Qiu, Y. Lu, Z. Wang, M. Wu, J. He and S. Shen, *Advanced Functional Materials*, 2021, **32**, 2106902.
8. M. Wei, X. L. Shi, Z. H. Zheng, F. Li, W. D. Liu, L. P. Xiang, Y. S. Xie, Y. X. Chen, J. Y. Duan, H. L. Ma, G. X. Liang, X. H. Zhang, P. Fan and Z. G. Chen, *Advanced Functional Materials*, 2022, **32**, 2207903.
9. D. Yang, X.-L. Shi, M. Li, M. Nisar, A. Mansoor, S. Chen, Y. Chen, F. Li, H. Ma, G. X. Liang, X. Zhang, W. Liu, P. Fan, Z. Zheng and Z.-G. Chen, *Nature Communications*, 2024, **15**, 923.